

In the format provided by the authors and unedited.

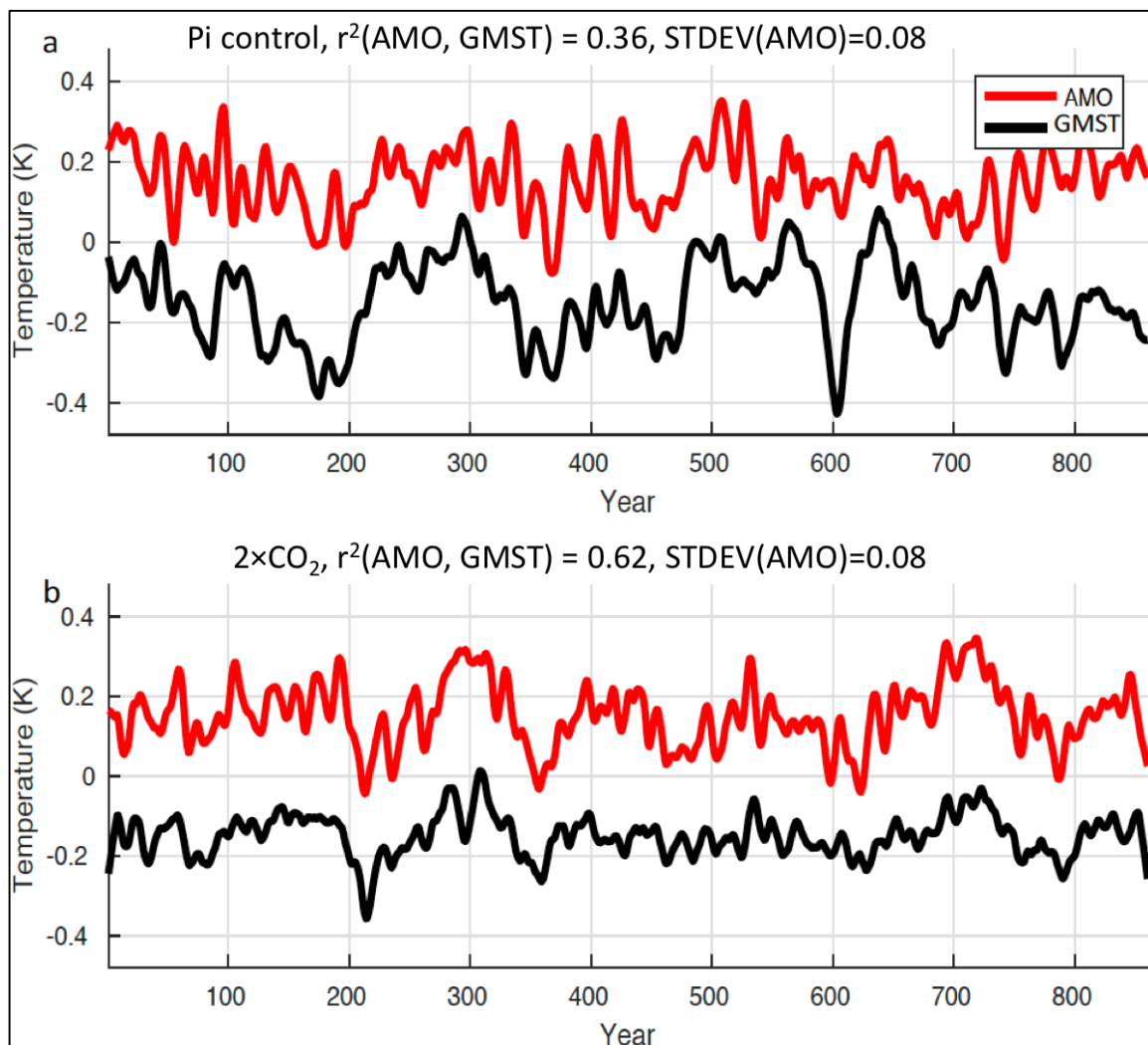
Change in the magnitude and mechanisms of global temperature variability with warming

Patrick T. Brown^{1*}, Yi Ming², Wenhong Li³ and Spencer A. Hill^{4,5}

¹Department of Global Ecology, Carnegie Institution for Science, Stanford, California 94305, USA. ²Geophysical Fluid Dynamics Laboratory/NOAA, Princeton, New Jersey 08540, USA. ³Earth and Ocean Sciences, Nicholas School of the Environment, Duke University, Durham, North Carolina 27708, USA. ⁴Department of Atmospheric and Oceanic Sciences, University of California, Los Angeles, California 90095, USA. ⁵Division of Geological and Planetary Sciences, California Institute of Technology, Pasadena, California 91125, USA. *e-mail: pbrown@carnegiescience.edu

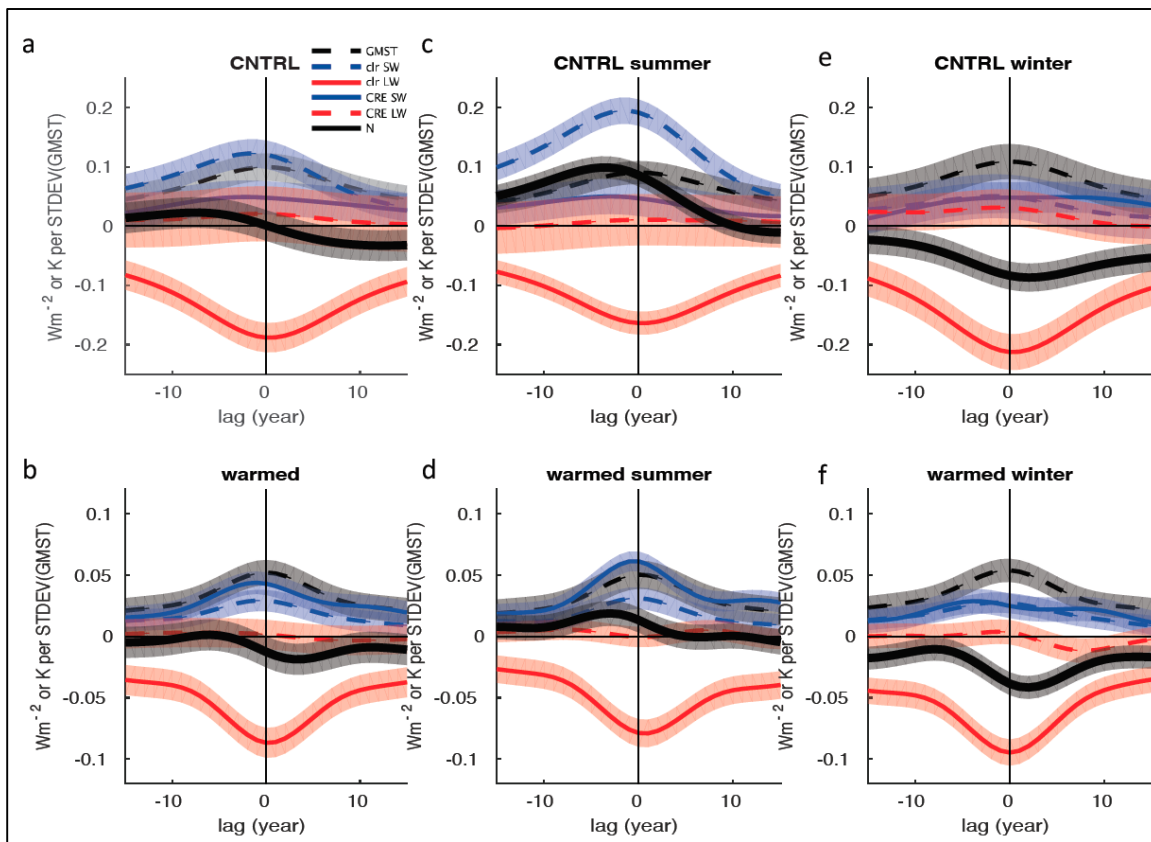
Supplementary Table 1. List of CMIP5 models used in this study.

| Model Name | Institution | Atmosphere Component Name | Atmosphere Resolution | Atmosphere Chemistry Component Name | Land Surface Component Name | Ocean Component Name | Ocean Resolution | Ocean Biogeo-Chemistry Component Name | Sea Ice Component Name |
|---------------|---|---------------------------|--|-------------------------------------|---------------------------------|-------------------------|---|---------------------------------------|--------------------------|
| bcc-csm1-1 | Beijing Climate Center, China Meteorological Administration | BCC_AGCM2.1 | T42 | N/A | BCC-AVIM1.0 | MOM4-L40 | 1° with enhanced resolution in the meridional direction in the tropics (1/3° meridional resolution at the equator) tripolar | Included | GFDL Sea Ice Simulator |
| CCSM4 | US National Centre for Atmospheric Research | CAM4 | 0.9° × 1.25° | N/A | Community Land Model 4 (CLM4) | POP2 with modifications | Nominal 1° (1.125° in longitude, 0.27°–0.64° variable in latitude) | N/A | CICE4 with modifications |
| CNRM-CM5 | Centre National de Recherches Meteorologiques and Centre Européen de Recherche et Formation Avancées en Calcul Scientifique | ARPEGE-Climat | TL127 | (3-D linear ozone chemistry model) | SURFEX (Land and Ocean Surface) | NEMO | 0.7° on average ORCA1 | PISCES | Gelato5 (Sea Ice) |
| CSIRO-Mk3-6-0 | Queensland Climate Change Centre of Excellence and Commonwealth Scientific and Industrial Research Organisation | Included | ~1.875° × 1.875° (spectral T63) | N/A | Included | Modified MOM2.2 | ~0.9 × 1.875 | N/A | Included |
| GISS-E2-H | NASA Goddard Institute for Space Studies USA | Included | 2° latitude × 2.5° longitude | G-PUCCINI | Included | HYCOM Ocean | 0.2 to 1° latitude × 1° longitude HYCOM | N/A | Included |
| GISS-E2-R | NASA Goddard Institute for Space Studies USA | Included | 2° latitude × 2.5° longitude | G-PUCCINI | Included | Russell Ocean | 1° latitude × 1.25° longitude Russell 1 × 1Q | N/A | Included |
| HadGEM2-ES | National Institute of Meteorological Research/Korea Meteorological Administration | HadGAM2 | 1.875° in longitude by 1.25° in latitude N96 | N/A | Included | Included | 1.875° in longitude by 1.25° in latitude N96 | N/A | Included |
| IPSL-CM5A-LR | Institut Pierre Simon Laplace | LMDZ5 | 96 × 95 equivalent to 1.9° × 3.75° LMDZ96 × 95 | N/A | Included | Included | 2 × 2-0.5° ORCA2 | PISCES | UIM2 |
| MPI-ESM-LR | Max Planck Institute for Meteorology | ECHAM6 | approx. 1.8° T63 | N/A | JSBACH | MPIOM | average 1.5° GR15 | HAMOCC | Included |

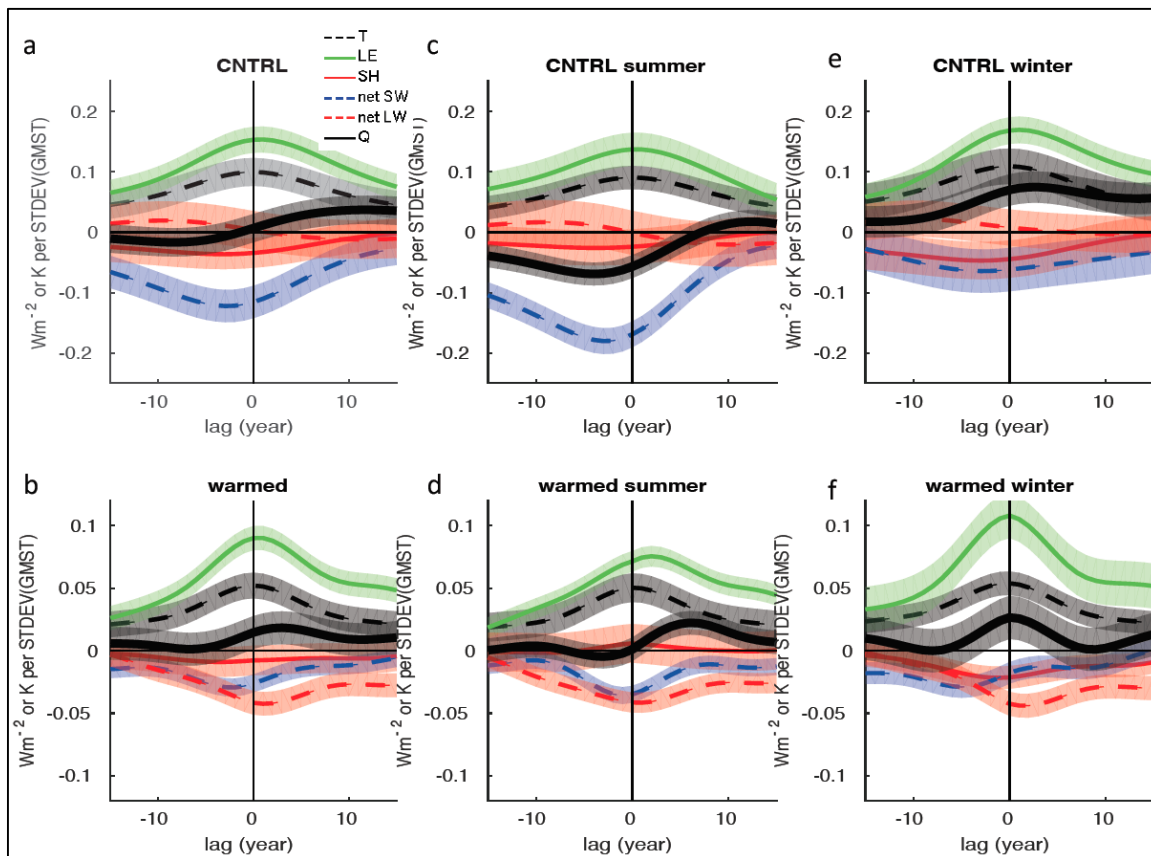


Supplementary Figure 1 | a, time series of the Atlantic Multidecadal Oscillation (AMO, spatially weighed mean SST from 7.5°W - 75°W and 0°N to 60°N) and GMST for the GFDL CM3 preindustrial control run. **b**, as in (a) but for the GFDL CM3 $2\times\text{CO}_2$ run. Time series are offset from 0 to allow for visual comparison.

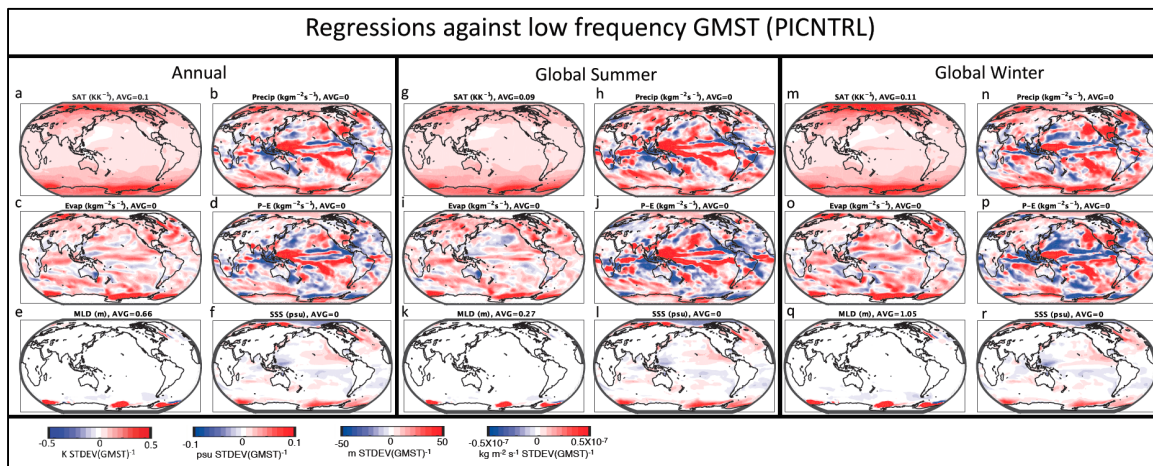
Seasonal Variability. Seasonally, the summer half-year is primarily responsible for producing the energy imbalances that enhance GMST variability in the preindustrial control run (Supplementary Fig. 2a). At TOA, the clear LW cooling and cloud components are not heavily dependent on season, so the difference between the summer half-year and winter half-year is primarily attributable to the clear SW component which is much more positive in the summer (cf. blue dashed line in Supplementary Figs. 2c and 2e). This relationship is also apparent at the surface, where the difference between winter and summer $\uparrow Q$ is primarily due to the net shortwave component (cf. blue dashed line in Supplementary Figs. 3c and 3e).



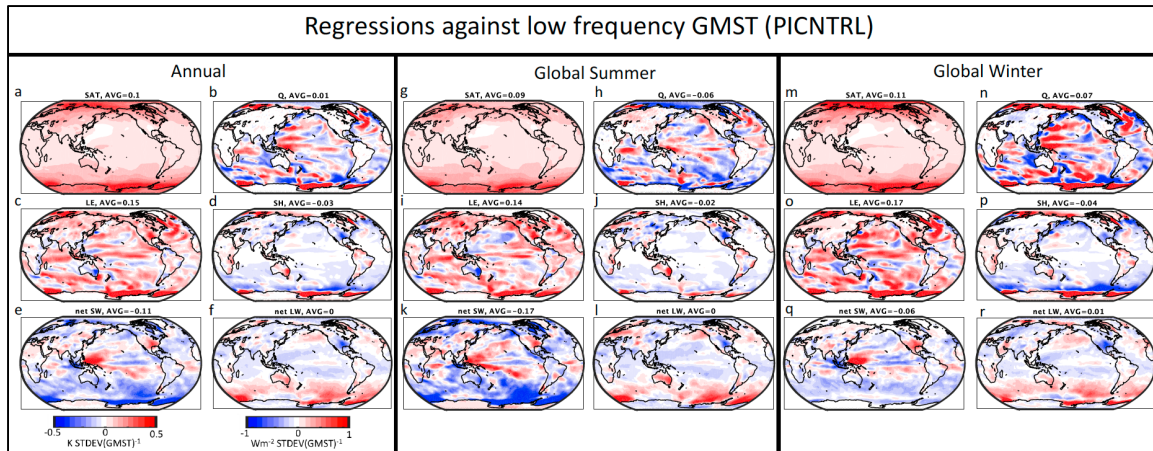
Supplementary Figure 2 | As in Fig. 2a and 2b but expanded seasonally. Here, seasons are global, meaning that the summer half-year for both hemispheres is considered simultaneously when producing the summer values and the winter half-year for both hemispheres is considered simultaneously to produce global winter values.



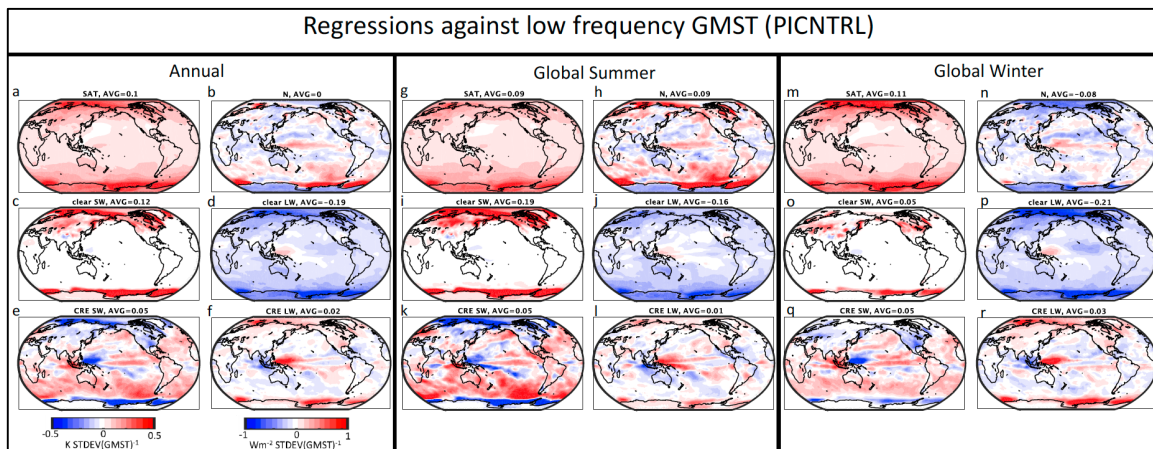
Supplementary Figure 3 | As in Fig. 2c and 2d but expanded seasonally. Here, seasons are global, meaning that the summer half-year for both hemispheres is considered simultaneously when producing the summer values and the winter half-year for both hemispheres is considered simultaneously to produce global winter values.



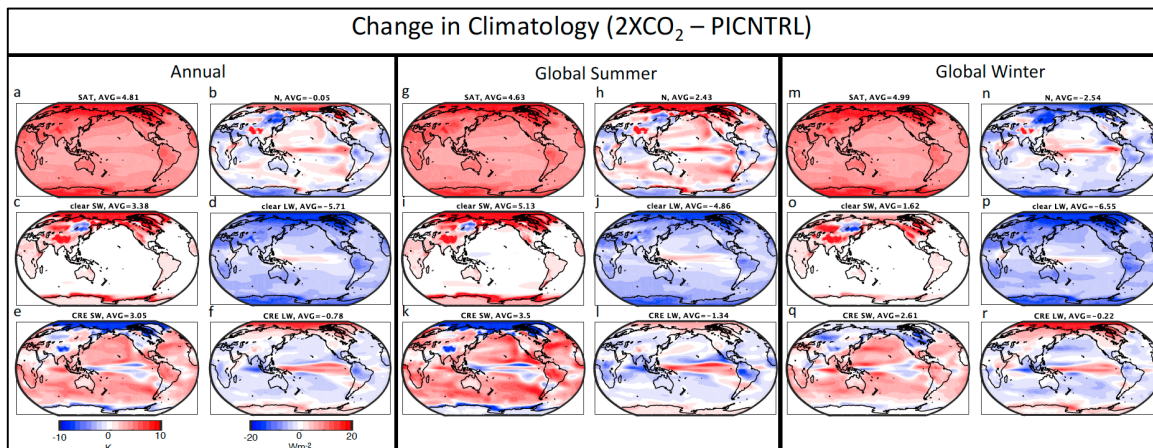
Supplementary Figure 4 | Regression of labeled variables against the standard deviation of GMST (not time lagged) in the GFDL CM3 preindustrial control run. MLD stands for mixed layer depth and SSS stands for sea surface salinity. Seasons are global, meaning that the summer half-year for both hemispheres is considered simultaneously when producing the summer values and the winter half-year for both hemispheres is considered simultaneously to produce global winter values.



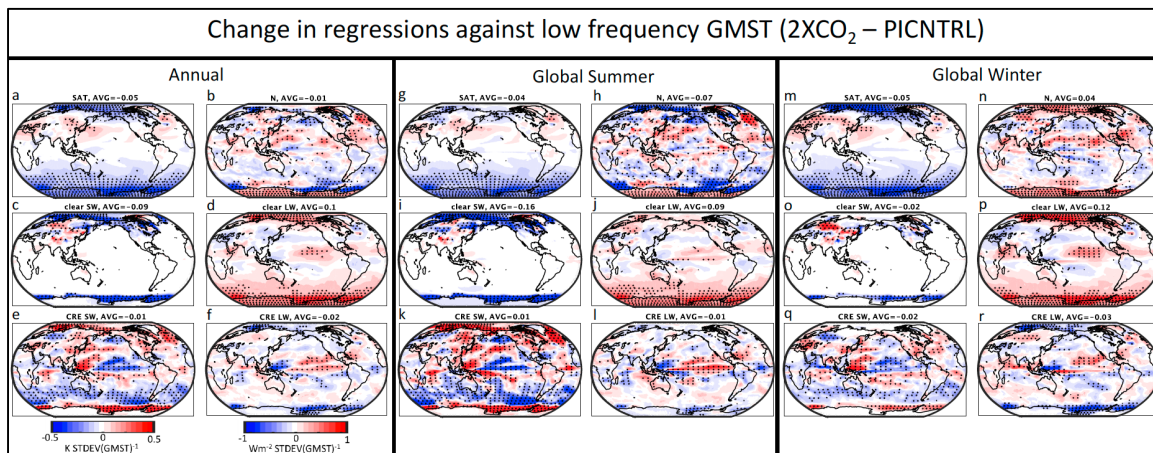
Supplementary Figure 5 | As in Supplementary Fig. 4 but with surface heat flux and its components.



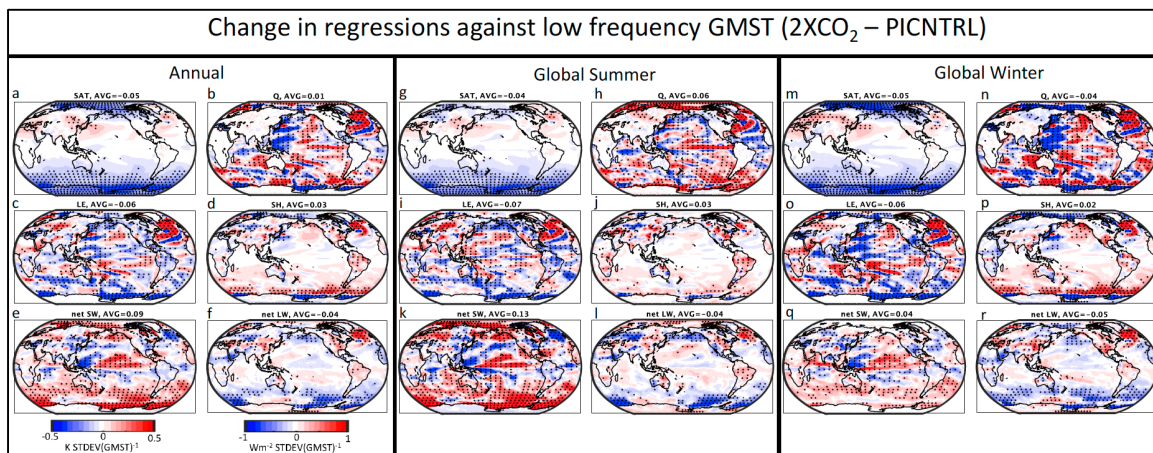
Supplementary Figure 6 | As in Supplementary Fig. 4 but with top-of-atmosphere radiative flux and its components.



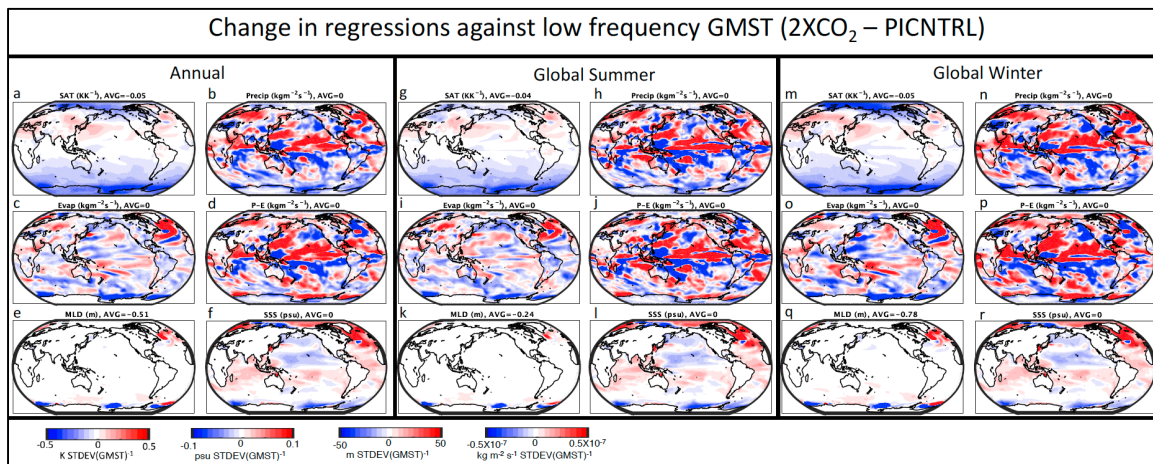
Supplementary Figure 7 | **a**, Change in annual mean climatological surface air temperature, **b**, net TOA flux, and **c-f**, four linearly additive components of TOA flux. **g-l**, as in **a-f** but for global summer. **m-r**, as in **a-f** but for global winter. Seasons are global, meaning that the summer half-year for both hemispheres is considered simultaneously when producing the summer values and the winter half-year for both hemispheres is considered simultaneously to produce global winter values.



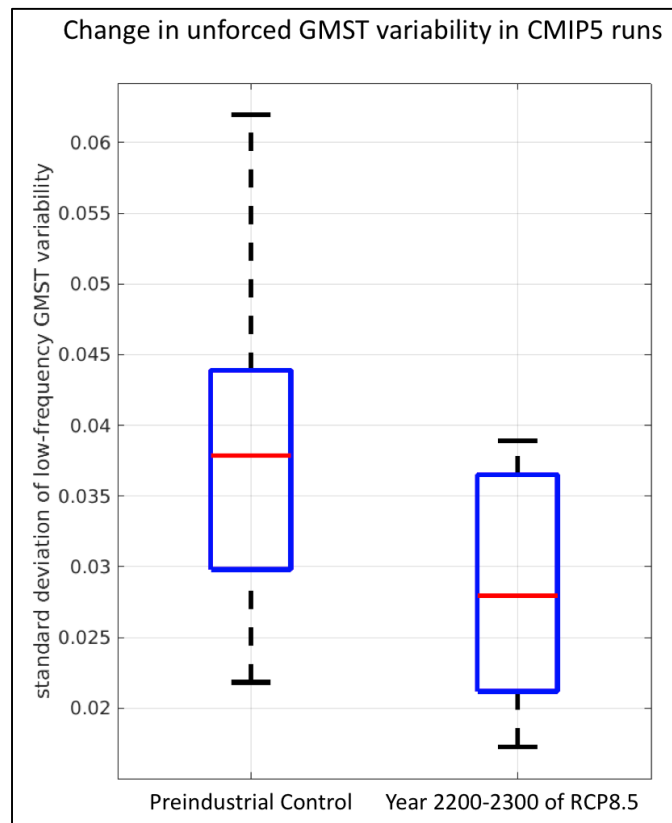
Supplementary Figure 8 | As in Fig. 3 but expanded seasonally. Seasons are global, meaning that the summer half-year for both hemispheres is considered simultaneously when producing the summer values and the winter half-year for both hemispheres is considered simultaneously to produce global winter values.



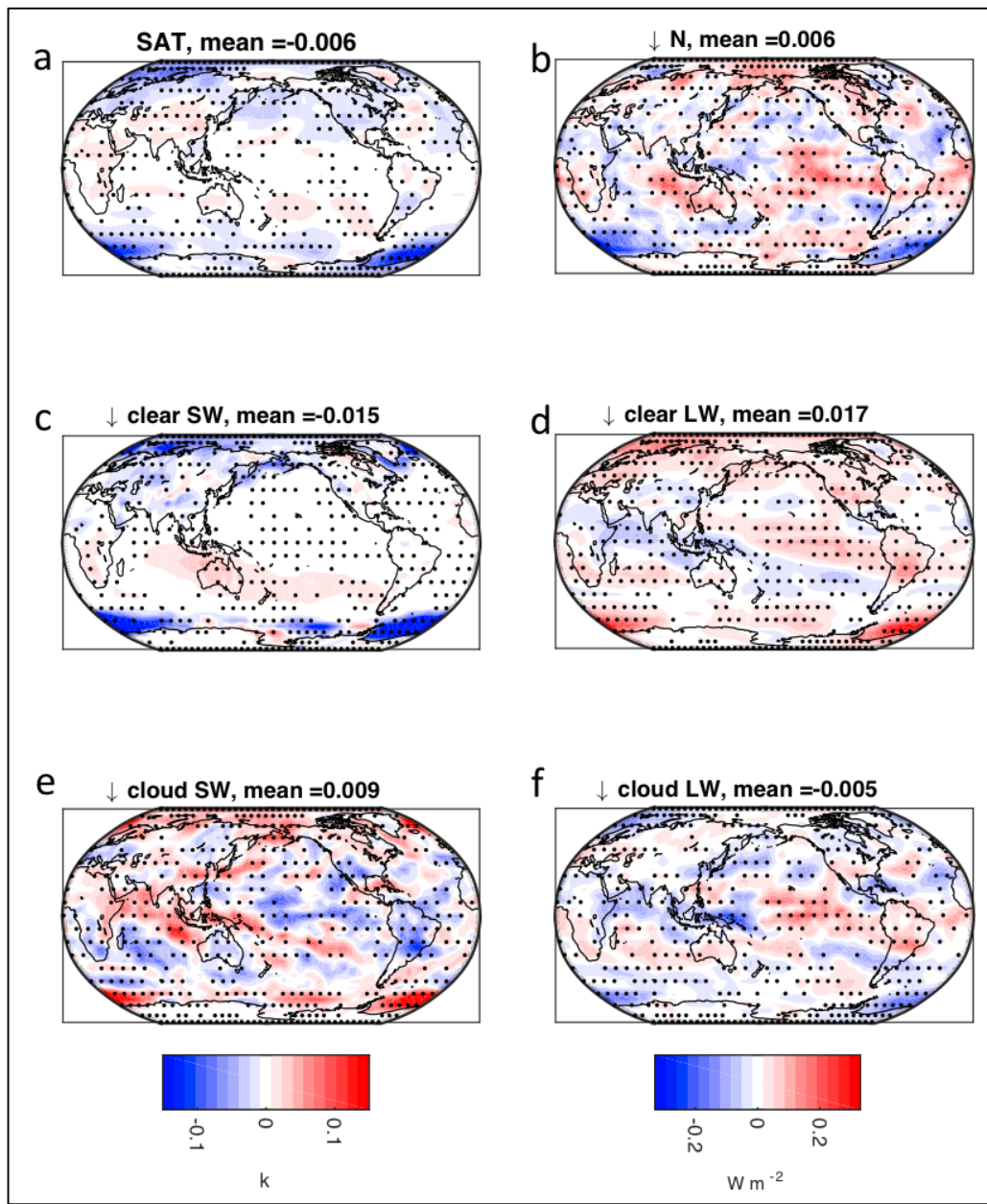
Supplementary Figure 9 | As in Supplementary Fig. 8 but with the surface energy budget instead of the TOA energy budget.



Supplementary Figure 10 | As in supplementary Fig. 8 but with additional variables labeled in the panels.

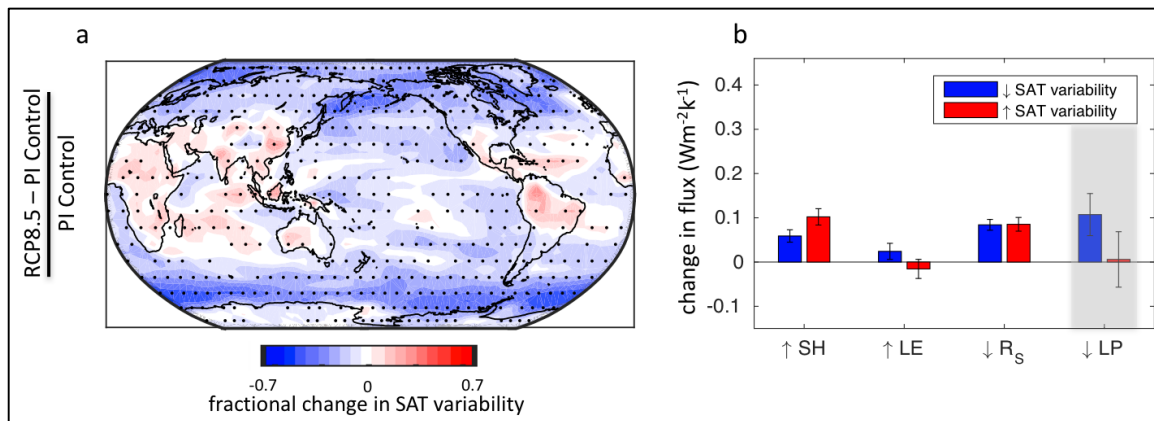


Supplementary Figure 11 | Box and whisker plots of low-frequency unforced GMST variability (temporal standard deviation) in CMIP5 models in their preindustrial control runs (left) and in their RCP8.5 runs from 2200-2300 (right). The horizontal red line is the model median, the box spans the 1st to the 3rd quartiles and the whiskers span the entire range. See Methods for the how unforced variability was isolated from forced variability in the RCP8.5 run. The ensemble mean standard deviation reduced by 26% between the two experiments and was statistically significant at the 90th percentile (p-value = 0.065) using a one-sided student's t-test assuming unequal variance.



Supplementary Figure 12 | As in Fig. 3 but using the multi-model mean regression coefficient difference in the CMIP5 models investigated (see Methods). CMIP5 models warmed more between their preindustrial control runs and the 2200-2300 time period of their RCP8.5 runs (8.1K on average) than the GFDL-CM3 model warmed between its preindustrial control and $2\times CO_2$ runs (4.81K). Thus, to make the above results comparable to Fig. 3, the values in the maps were multiplied by a deflation factor

($4.81\text{K}/8.1\text{K}=0.59$). Note that the color scale is narrower than in Fig. 3 partially because averaging over positive and negative values from different models results in smaller magnitudes. Stippling represents where at least six out of nine models agreed on the sign change of the regression coefficient.



Supplementary Figure 13 | As in Fig. 4a and 4b but using the multi-model mean difference in the CMIP5 models investigated (see Methods). Stippling in (a) represents where at least six out of nine of the models agreed on the sign of the change in the magnitude of low frequency SAT variability. CMIP5 models warmed more between their preindustrial control runs and the 2200-2300 time period of their RCP8.5 runs (8.1K on average) than the GFDL-CM3 model warmed between its preindustrial control and 2 \times CO₂ run (4.81K). Thus, to make Supplementary Fig. 13a comparable to Fig. 4a, the values in the maps were multiplied by a deflation factor ($4.81\text{K}/8.1\text{K}=0.59$).